Neurobiology of Disease

Mechanisms of Fast Ripples in the Hippocampus

Volodymyr I. Dzhala and Kevin J. Staley
Department of Neurology and Pediatrics, University of Colorado Health Sciences Center, Denver, Colorado 80262

Hippocampal fast ripples (FRs) have been associated with seizure onset in both human and experimental epilepsy. To characterize the mechanisms underlying FR oscillations (200–600 Hz), we studied activity of single neurons and neuronal networks in rat hippocampal slices *in vitro*. The correlation between the action potentials of bursting pyramidal cells and local field potential oscillations suggests that synchronous onset of action potential bursts and similar intrinsic firing patterns among local neurons are both necessary conditions for FR oscillations. Increasing the fidelity of individual pyramidal cell spike train timing by blocking accommodation dramatically increased FR amplitude, whereas blockade of potassium conductances decreased the fidelity of action potential timing in individual pyramidal cell action potential bursts and decreased FR amplitude. Blockade of ionotropic glutamate receptors desynchronized onset of action potential bursts in individual pyramidal cells and abolished fast ripples. Thus, synchronous burst onset mediated by recurrent excitatory synaptic transmission and similar intrinsic spike timing mechanisms in neighboring pyramidal cells are necessary conditions for FR oscillations within the hippocampal network.

Key words: **fast ripples; hippocampus; CA3; glutamate receptors; epilepsy; rhythm; gamma**

Introduction

Coherent oscillations, in which populations of neurones fire in a synchronous and periodic manner, are thought to be important in higher brain functions. Several patterns of synchronized neuronal activity are present in the hippocampus, including theta rhythm (4–10 Hz), gamma-frequency oscillations (20–100 Hz), and sharp-wave-associated high-frequency oscillations (~200 Hz) (Vanderwolf, 1969; Buzsaki, 1986; Bragin et al., 1995; Ylinen et al., 1995). Theta and gamma oscillations critically depend on the time course of synaptic inhibition by GABAergic interneurons, which coordinate the activity of pyramidal cells (Cobb et al., 1995). Sharp wave bursts, induced by a cooperative discharge of CA3 pyramidal cells, are the most synchronous normal electroencephalographic (EEG) pattern in the hippocampus. During sharp wave discharges observed in *in vivo* models, CA3 neurones fire synchronous bursts of action potentials that produce high-frequency (~200 Hz) oscillations in the CA1 region (Ylinen et al., 1995). High-frequency oscillations occur predominantly in the CA1 pyramidal cell layer, usually superimposed on the negative phase of sharp waves, and last tens of milliseconds.

Recent electrophysiological studies in kainic acid-treated rats have revealed high-frequency (200–600 Hz) oscillations, termed fast ripples (FRs) (Bragin et al., 1999c, 2002). They appeared to reflect field oscillations composed of hypersynchronous action potentials and may be an EEG analog of epileptiform discharges consisting of bursts of population spikes (Andersen et al., 1971; Bragin at al., 1999b). These oscillations uniquely occur in areas that generate spontaneous seizures. Two similar types of high-frequency field oscillations have been recorded from the entorhinal cortex and hippocampus of patients with medial temporal lobe epilepsy (Bragin et al., 1999a). The first type appears to be the human equivalent of normal ripples in the rat. The second, fast ripples in the frequency range of 250–600 Hz, are found in the epileptogenic region and may reflect pathological hypersynchronous population spikes of bursting pyramidal cells. In addition, several studies demonstrated that high-frequency oscillations sometimes precede the onset of focal seizures (Fisher et al., 1992; Bragin et al., 1999a; Traub et al., 2001).

The mechanisms and principles that underlie the period of high-frequency oscillations in the hippocampus are controversial. *In vivo* study suggests (Ylinen et al., 1995) that field oscillations in the ~200 Hz frequency band in the CA1 region reflect summed IPSPs in pyramidal cells as a result of high-frequency barrage of interneurons. However, *in vitro* studies demonstrate (Draguhn et al., 1998; Traub et al., 2001; Bikson et al., 2003; LeBeau et al., 2003) that synchronous network activity in this frequency range is not mediated through the more commonly studied modes of chemical synaptic transmission, but is in fact a result of direct electrotonic coupling of neurons, most likely through axon-axonal gap-junction connections.

The goal of our investigations was to characterize the mechanisms that determine the generation and timing of 200–600 Hz oscillations in the hippocampus. We measured activity of single pyramidal cells within population of neurons using simultaneous cell-attached recordings and extracellular electrode arrays in the hippocampal slice preparation *in vitro* to reveal the cellular-synaptic origin of the fast ripple oscillations.

Materials and Methods

Experimental system. Experiments were performed on hippocampal slices of postnatal day 12–30 (P12–P30) male Wistar rats. All animal use protocols conformed to the National Institutes of Health guidelines and

Received April 27, 2004; revised Aug. 31, 2004; accepted Sept. 1, 2004.

This work was supported by a grant from the National Institutes of Health–National Institute of Neurological Disorders and Stroke.

Correspondence should be addressed to Kevin J. Staley, Department of Neurology and Pediatrics, University of Colorado Health Sciences Center, 4200 East Ninth Avenue, B182, Denver, CO 80262. E-mail: Kevin.Staley@UCHSC.edu.

DOI:10.1523/JNEUROSCI.3112-04.2004

 0270-6474/04/248896-11$15.00/0

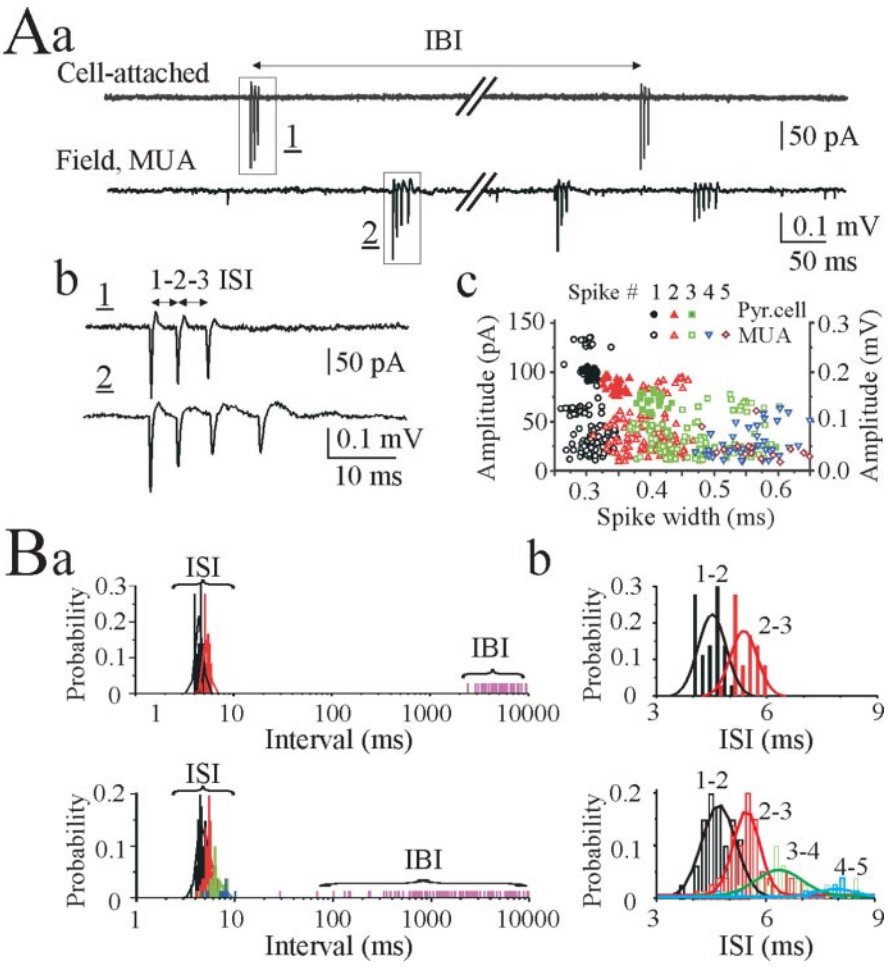

Figure 1. Spontaneous burst-type action-potential activity of CA3 pyramidal cells. *Aa*, Simultaneous cell-attached recording from the CA3 pyramidal cell (top trace) and 200-μm-apart extracellular field potential recording (bottom trace) of multiple unit activity in the CA3 pyramidal cell layer in a P20 rat hippocampal slice *in vitro*. Spontaneous bursts of action potentials are present in both records. *Ab*, Spontaneous bursts from cell-attached and extracellular recordings shown on an expanded time scale. *Ac*, Intraburst spike amplitude and spike width distributions from the cell-attached record (78 spikes in 29 bursts) and extracellular record of multiple unit activity (266 spikes in 101 bursts). In both records, intraburst spike amplitude proportionally decreased and spike width proportionally increased. *Ba*, Distributions of ISIs (bin size, 0.2 msec) and interburst intervals (IBI) from simultaneous cell-attached recording from the CA3 pyramidal cell (top graph) and extracellular recording of multiple unit activity in the CA3 pyramidal cell (bottom graph). Two distributions are clearly separable, and the ISIs are similar for the individual pyramidal cell bursts [4.5 $\pm$ 0.05 msec (1–2 ISI) and 5.4 $\pm$ 0.06 msec (2–3 ISI)] and multiple unit burst activity [4.7 $\pm$ 0.05 msec (1–2 ISI) and 5.6 $\pm$ 0.08 msec (2–3 ISI)]. *Bb*, ISI distributions from *Ba*. A Gaussian equation was used to fit a curve to the active data plots.

University of Colorado Health Sciences Center animal care on the use of laboratory animals. Animals were anesthetized and decapitated. After dissection, the brain was rapidly removed and placed in oxygenated (95% O_2–5% CO_2) ice-cold artificial CSF (aCSF) of the following composition (in mM): 126 NaCl, 3.5 KCl, 2.0 $CaCl_2$, 1.3 $MgCl_2$, 25 $NaHCO_3$, 1.2 NaH_2PO_4, and 11 glucose, pH 7.4. Hippocampal transverse slices (thickness, 450 μm) were cut using Leica VT-1000E vibratome (Leica, Nussloch, Germany) and kept in oxygenated aCSF at room temperature for at least 1 hr before use. Hippocampal slices posterior to the midtemporal (caudal) part of the hippocampus (plates 100–109; according to Paxinos and Watson, 1986) were used in this study.

Electrophysiology and data analysis. For electrophysiological recordings, individual slices were transferred to a conventional submerged-type chamber and continuously superfused with oxygenated aCSF at 32°C and at a rate of 2–3 ml/min. Cell-attached and whole-cell recordings were made using an Axopatch 200 and MultiClamp 700B amplifiers (Axon Instruments, Foster City, CA). Infrared-differential interference contrast microscopy (Axioscop FS; Zeiss, Oberkochen, Germany) through a 40× water immersion objective was used for visual control of some experiments. Patch electrodes were made from borosilicate glass capillaries (G150F-4; Warner Instruments, Hamden, CT) using the model P-97 Flaming-Brown micropipette puller (Sutter Instruments, Novato, CA). For cell-attached recording, pipettes were filled with aCSF or with solution containing (in mM): 135 cesium-gluconate, 2 $MgCl_2$, 0.1 $CaCl_2$, 1 EGTA, 2 Na_2ATP, and 10 HEPES, pH 7.25. For whole-cell recording in current-clamp mode, pipettes were filled with solution containing (in mM): 135 potassium gluconate, 2 $MgCl_2$, 0.1 $CaCl_2$, 1 EGTA, 2 Na_2ATP, and 10 HEPES, pH 7.25.

Extracellular field potentials were recorded using tungsten microelectrodes and a low-noise [<5 μV root mean square (RMS); referred to input] multichannel amplifier (bandpass, 0.1–4 kHz; 1000×). Microelectrodes made from coated tungsten wire of 50 μm diameter (California Fine Wire Company, Grover Beach, CA) were used for simultaneous recordings of multiple unit activity (MUA) (500 Hz high-pass filter), population field activity in EEG band (1–100 Hz), and fast ripple oscillations (200–600 Hz). RMS noise level with an electrode placed in the perfusion solution was typically 4–5 μV, whereas the amplitude of action potentials recorded from the stratum pyramidale ranged from this noise level up to 200 μV. The signals were digitized using an analog-to-digital converter (DigiData 1322A; Axon Instruments). Sampling interval per signal was 100 μsec (10 kHz). pCLAMP 9.2 (Axon Instruments), Mini Analysis 5.6 (Synaptosoft, Decatur, GA), and Origin 5.0 (Microcal Software, Northampton, MA) programs were used for the acquisition and data analysis. Power spectrum analysis was performed after applying a Hamming window function. Power was calculated by integrating the RMS value of the signal in frequency bands from 1 to 600 Hz (EEG and fast ripple band) and from 200 to 600 Hz (fast ripple band). The multiple unit activity was determined from high-pass filtered (500 Hz) raw data with a spike detection algorithm (Mini Analysis Program) and verified visually. Spikes with amplitude >three times the root mean square noise level were accepted.

Group measures were expressed as mean $\pm$ SEM; error bars also indicate SEM. The statistical significance of differences was assessed with Student's *t* test. The level of significance was set at $p < 0.05$.

Drugs. Reagents were purchased from Sigma (St. Louis, MO) and Tocris Cookson(Ellisville, MO), prepared as stock solutions, and stored aliquoted in tightly sealed vials at the manufacturer's recommended temperatures. During the experiments, thawed aliquots were kept on ice and protected from light until use.

Results

Spontaneous bursting activity of hippocampal neurons

CA3 pyramidal cells were studied in P12–P30 rat hippocampal slices using simultaneous cell-attached recordings from single pyramidal cells and local field potential recordings of MUA from the pyramidal cell layer (Fig. 1*A*). In cell-attached recordings, 22% of CA3 pyramidal cells (10 from 46) spontaneously generated action potentials (spikes), either as single spikes or burst of spikes. Burst-type discharges from pyramidal cells were characterized by variable numbers (from two to six) of intraburst spikes and 4–10 msec intraburst interspike intervals (ISIs) with modest

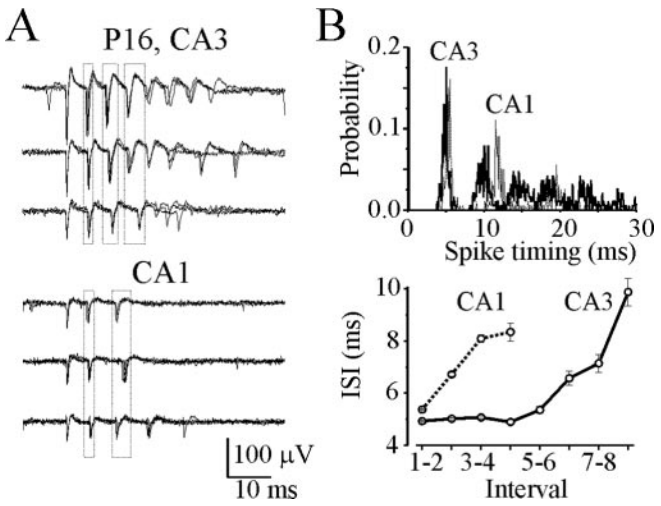

Figure 2. Spatial distribution of the intraburst ISIs. *A*, Simultaneous extracellular field potential records of multiple unit activity were made in the stratum pyramidale of the CA3 and CA1 areas in a P16 hippocampal slice. Spontaneous burst-type discharges of individual neurons were extracted from continuous extracellular records. Rows of superimposed traces represent burst-type discharges of three individual neurons in the CA3a (top traces) and three individual neurons in the CA1 (bottom traces) pyramidal cell layer. Outlined areas indicate the range of timing for consecutive intraburst spikes. *B*, Histograms (top graph) represent spike timing in all detected burst-type discharges recorded from the CA3a (1105 spikes in 190 bursts) and CA1 (727 spikes in 200 bursts) pyramidal cell layer (bin size, 0.1 msec). Plot below shows significant differences of the corresponded intraburst interspike intervals: 4.9 ± 0.03 msec (1–2 ISI in CA3) and 5.4 ± 0.03 msec (1–2 ISI in CA1; $p = 1.97 \times 10^{-21}$).

accommodation. Gradually decreasing amplitude and increasing width characterized intraburst spikes (Fig. 1*A*). Individual pyramidal cells sustained remarkably stereotyped ISIs over long periods of time (Fig. 1*B*). Interburst intervals for spontaneously bursting pyramidal cells varied from seconds to minutes, indicating a random burst onset (Fig. 1*B*).

In simultaneous extracellular records from the CA3 pyramidal cell layer (Fig. 1*A*), spontaneous and irregular bursts of two to eight spikes were always apparent. Spike amplitude ranged from the noise level up to 100–300 μV, suggesting that electrodes detected activity from hundreds of single neurons simultaneously (Cohen and Miles, 2000; Dzhala and Staley, 2003a,b). In hippocampal slices from P20 rats, ISIs increased from 4–5 msec between spikes 1 and 2 (1–2 ISI) to 6–10 msec between spikes 3–4 and 4–5 (3–4; 4–5 ISIs), corresponding to the spike frequency adaptation seen in cell-attached recordings (Fig. 1*A*,*B*). Descending amplitude and increasing width, similar to the intraburst spikes from cell-attached recordings, characterized intraburst spikes from extracellular records of multiple unit activity (Fig. 1*A*).

Spontaneous bursts of action potentials could also be observed in the CA1 pyramidal cell layer (Fig. 2*A*). Using spike-detecting and burst-analyzing algorithms (Abeles and Gerstein, 1988), we separated the complex firing patterns of individual neurons from the discharges of ensembles of neurons (Fig. 2*A*). Spontaneous bursts of action potentials recorded from neurons within area CA3 were similar, and bursts of action potentials recorded from neurons within area CA1 were similar ($n = 15$ slices). However, when bursts from neurons in the two subregions were compared, bursts from the two regions significantly differed in duration, number of intraburst spikes, and intraburst ISIs, suggesting a spatially distinct pacemaker activity along the pyramidal cell layer (Fig. 2*A*,*B*).

Thus, a proportion of pyramidal cells in the rat hippocampal slices *in vitro* spontaneously generate burst-type discharges characterized by random burst onset and similar ISIs, but these ISIs vary between hippocampal subregions. If fast ripples were composed of the synchronous onset of burst activity in local ensembles of neurons, the fast ripple activity would be expected to vary with hippocampal subregions.

Fast ripple oscillations

Modulation of extracellular potassium concentration $[K^+]_o$ has a profound impact on the excitability of neurons and neuronal networks. In the CA3 region of the rat hippocampus, synchronized population bursts occurred in conditions of increased $[K^+]_o$ and spread bidirectionally into CA1 and dentate gyrus (Traynelis and Dingledine, 1988; Jensen and Yaari, 1997; Dzhala and Staley, 2003a,b). We used dual cell-attached recordings from the CA3 pyramidal cells, as well as simultaneous cell-attached recordings from the CA3 pyramidal cells and nearby extracellular field potential recordings of multiple unit activity and population activity in the stratum pyramidale of the CA3 region, to study the relationship between single cell action potentials, multiple unit activity, and population field activity (Fig. 3-6) as neuronal activity became synchronized in 8.5 mM $[K^+]_o$.

Increasing the extracellular concentration of potassium progressively increased the firing rate of spontaneously active cells as well as recruitment of previously inactive cells to generate action potentials (Cohen and Miles, 2000; Dzhala and Staley, 2003b). Cell-attached recordings demonstrate that 94% of CA3 pyramidal cells (43 from 46) generated bursts of action potentials in the presence of high extracellular potassium. Interburst intervals after 8.5 mM $[K^+]_o$ application became periodic and decreased to 1.72 ± 0.2 sec at P15–P20 ($n = 12$) and 3.4 ± 0.3 sec at P25–P30 ($n = 8$). The number of intraburst spikes in individual CA3 pyramidal cells increased from 2–6 to 5–20, and intraburst ISIs decreased by 10–50% (Fig. 3*B*). Dual cell-attached recordings ($n = 6$) from neighboring CA3 pyramidal cells revealed progressive burst synchronization after 8.5 mM $[K^+]_o$ application. The time delay between burst onsets in two pyramidal cells progressively decreased, trending to zero (Fig. 3*C*). Neighboring pyramidal cells demonstrated similar intraburst interspike intervals with a progressive reduction of firing frequency during the burst (spike frequency adaptation) (Figs. 3*C*, 4). Cross-correlation analysis of the intraburst spike timing revealed high-frequency oscillations with a period of 3–10 msec (100–350 Hz) (Fig. 4).

Simultaneous extracellular electrode array recordings of multiple unit activity revealed a dramatic increase of neuronal discharges in all recording areas (Fig. 5*A*). Interburst intervals for multiple neuron activity after 8.5 mM $[K^+]_o$ application progressively decreased, trending to zero (Fig. 5*Ba*). Amplitude histograms for spontaneous multiple unit activity exhibited several peaks in control conditions and were smoothed in the presence of 8.5 mM $[K^+]_o$, suggesting recruitment of numerous new neurons to generate action potentials (Fig. 5*Bb*). Intraburst ISIs for MUA after 8.5 mM $[K^+]_o$ application decreased to 82.6 ± 1.1% of control ($n = 8$) (Fig. 5*C*). Synchronization of neuronal discharges eventually resulted in high-amplitude network-driven population bursts (Fig. 5*A–C*).

These population bursts had the typical features of interictal epileptiform discharges (IEDs) (Pedley, 1980; Dzhala and Staley, 2003b). Fast Fourier transform filtering within specific bandwidths revealed low-frequency field potential oscillations in the EEG band (1–100 Hz), high-frequency population spikes in the fast ripple band (100–500 Hz), and multiple unit activity in the highest frequency windows (500–1000 Hz) (Fig. 6*A*). Ampli-

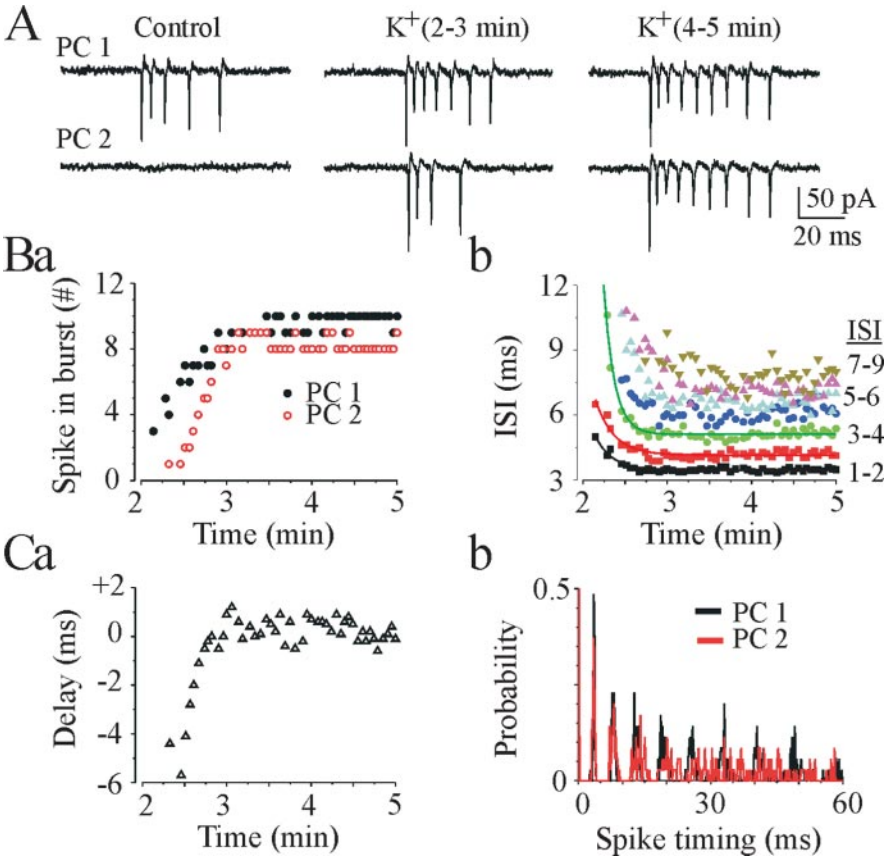

Figure 3. Effects of 8.5 mM $[K^+]_o$ on spontaneous burst-type discharges. *A*, Dual cell-attached recordings from neighboring CA3 pyramidal cells (PC1 and PC2) in a P18 rat hippocampal slice. Bath application of 8.5 mM $[K^+]_o$ increased neuronal firing rate and decreased time delay between burst onset in individual pyramidal cells, resulting in their synchronization. *Ba*,*b*, The number of intraburst spikes in the CA3 pyramidal cells (PC1 and PC2) progressively increased and the intraburst interspike intervals (PC1) progressively decreased after 8.5 mM $[K^+]_o$ application. Time axis starts 2 min after 8.5 mM $[K^+]_o$ application. *Ca*, Time delay between two pyramidal cell burst onset after 8.5 mM $[K^+]_o$ application progressively decreased, tending to zero. *Cb*, Three minutes after high $[K^+]_o$ application, two neighboring pyramidal cells sustained hypersynchronous bursts characterized by similar intraburst interspike intervals (326 spikes in 35 bursts for PC1 and 281 spikes in 35 bursts for PC2; bin size, 0.2 msec).

tudes of population spikes varied from 0.1 to 1.5 mV, and their width varied from 0.6 to 3 msec (Fig. 6*B*). Individual pyramidal cells generated action potentials during population bursts with a probability of 0.96 ± 0.02 ($n = 14$). The number of spikes generated by individual neurons during population bursts varied from 5 to 28, and their firing was phase locked to the fast ripple oscillations. Cross-correlation analysis of the population spike timing and multiple unit activity relative to the single pyramidal cell spike timing revealed coherent high-frequency oscillations with a period of 3–8 msec (125–350 Hz) in the P20 rat hippocampal slices (Fig. 6*B*).

Power spectra analysis of population activity recorded simultaneously from the CA3 and CA1 pyramidal cell layers revealed a wider bandwidth and higher frequency of peak power for the FR oscillations in the CA3 versus CA1 areas ($n = 10$) (Fig. 7*A*). These differences correspond to the differences seen in bursts of action potentials from individual pyramidal cells in these regions, supporting the idea that the coherent onset of burst activity in a local ensemble of neurons may underlie fast ripple generation.

We demonstrated previously that power in the FR oscillation band increased preictally in this preparation (Dzhala and Staley, 2003b). We measured the amplitude and frequency of fast ripple oscillations as neuronal activity became synchronized by high potassium and before transition to ictal-like epileptiform activity in the P12–P16 rat hippocampal slices. FR amplitude progressively increased after the appearance of synchronized population bursts ($n = 10$) (Fig. 7*B*). Before onset of ictal activity, fast ripple oscillations were often followed by secondary afterdischarges at intervals of 30–100 msec (gamma-tail complex). Secondary afterdischarges were characterized by slower 100–150 Hz population spikes (Fig. 7*B*), consistent with the preictal observations in human (Fisher et al., 1992) and experimental epilepsy (Bragin et al., 1999c).

These results suggest that two conditions are associated with the occurrence of fast ripple oscillations in the hippocampal network: synchronous onset of action potential bursts and similar intraburst spike timing in regional pyramidal cells.

Contribution of intrinsic cellular properties to the timing of fast ripple oscillations

Both synaptic activities and intrinsic membrane properties underlie much of the spontaneous activity of pyramidal cells in the hippocampus *in vitro* (Cohen and Miles, 2000). To determine the mechanisms underlying the homogenous intraburst spike timing, we studied whether alterations of intrinsic membrane properties altered spike timing in single cell bursts and the consequent effects on synchronous population activity.

As a first approach, we analyzed the influence of slow afterhyperpolarizing potassium current (I_{AHP}), delayed rectifier potassium current (I_{Kd}), and hyperpolarization activated cation current (I_h) (McCormick, 1990; Storm, 1990) on the intraburst action potential timing using cell-attached and whole-cell current-clamp recordings from CA3 pyramidal cells (Fig. 8).

I_{AHP} significantly contributes to the tendency of the firing frequency of hippocampal pyramidal neurons to decrease during maintained depolarization, a process known as spike frequency adaptation (Madison and Nicoll, 1986). Suppression of I_{AHP} with norepinephrine (20 μM) decreased the intraburst interspike intervals in CA3 pyramidal cells by 8.3 ± 3.2% ($n = 6$; $p = 0.03$) (Fig. 8*A*) and decreased ISI variance by 20.1 ± 18% ($p = 0.28$).

Blockade of I_{Kd} by bath application of TEA^+ (2 mM) significantly increased spontaneous burst duration and altered stereotyped intraburst interspike intervals (Fig. 8*B*). The average ISIs in sequential bursts recorded from individual neurons increased by 202 ± 64% ($n = 6$; $p = 0.005$) (Fig. 8*B*), and ISI variance increased by >1000-fold.

Similar changes of the intraburst ISIs and ISI variance in bursting pyramidal cells were observed after blockade of I_h by bath application of Cs^+ (3 mM). Intraburst ISIs increased by 6.1 ± 1.9% ($n = 6$; $p = 0.018$) (Fig. 8*C*), and ISI variance increased by 282 ± 74% ($p = 0.009$).

Thus, the intrinsic membrane properties strongly contribute to the intraburst spike timing mechanisms and determine a vari-

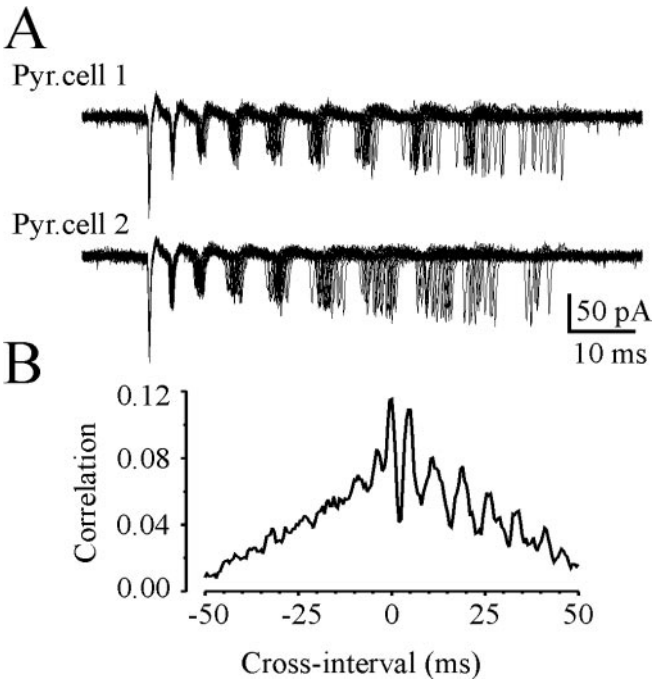

Figure 4. Synchrony of CA3 pyramidal cell oscillators. *A*, Dual cell-attached recordings from neighboring CA3 pyramidal cells (PC1 and PC2) in a P18 rat hippocampal slice after 8.5 mM $[K^+]_o$ application. Superimposed traces of 25 consecutive bursts illustrate synchronous burst onset and increasing of the spike-to-spike interval variance as a consequence of spike frequency adaptation. *B*, Cross-correlation analysis of the intraburst spike timing (bin size, 0.5 msec) reveals high-frequency oscillations with a period of 3–10 msec (100–350 Hz).

ety of burst characteristics from the frequency of intraburst firing to the slow adaptation of action potential frequency.

Next, we measured activity of single pyramidal cells within a population of neurons using simultaneous cell-attached recordings and extracellular electrode arrays in the hippocampal slice preparation *in vitro* and analyzed the influence of I_{AHP}, I_{Kd}, and I_h currents on the ISIs of CA3 pyramidal cells and timing of fast ripple oscillations (Fig. 9).

Blockade of I_{AHP} reduces spike train accommodation and thereby increases the fidelity of spike timing during bursts of action potentials in hippocampal pyramidal cells (Madison and Nicoll, 1986). In the presence of 8.5 mM $[K^+]_o$, single cell intraburst discharges were hypersynchronous with high-frequency population spikes related to FR oscillations ($n = 6$) (Fig. 9*A*). Bath application of the I_{AHP} blocker norepinephrine (20 μM) decreased intraburst interspike intervals (ISI 1–2; 2–3; 3–4) by 12.1 ± 2% ($n = 5$ of 6; $p = 0.01$) and ISI variance by 44 ± 17% ($p = 0.02$) in bursting pyramidal cells. There was a corresponding increase in the power spectra amplitude and frequency range relating to the fast ripples (Fig. 9*A*). Power spectra amplitude increased by 67 ± 27% ($p = 0.04$), and peak of FR frequency increased by 3.9 ± 1.6% ($n = 6$; $p = 0.044$).

Blockade of I_{Kd} by bath application of TEA^+ (2 mM) strongly increased intraburst interspike intervals by 86 ± 15% ($n = 6$; $p = 0.0001$) and ISI variance by >100-fold ($p = 0.03$). There was a corresponding decrease in coherence between action potentials of bursting pyramidal cells and local extracellular field potentials, resulting in a suppression of power spectra amplitude (Fig. 9*B*). Power spectra amplitude decreased by 51.4 ± 13% ($p = 0.018$), and peak of FR frequency decreased by 26.75 ± 1% ($p = 1.7 \times 10^{-7}$).

Similar changes of the intraburst ISIs and ISI variance in bursting pyramidal cells were observed after blockade of I_h by bath application of Cs^+ (3 mM). Intraburst ISIs increased by 26.5 ± 15% ($n = 6$; $p = 0.11$), and ISI variance increased by 966.5 ± 479% ($p = 0.08$), resulting in decrease in the power spectra amplitude in the frequency range relating to the fast ripples (Fig. 9*C*). Power spectra amplitude decreased by 29.7 ± 15.3% ($p = 0.07$), and peak of FR frequency decreased by 25.3 ± 5.5% ($p = 0.001$). Another I_h current blocker, ZD7288 (4-ethylphenylamino-1,2-dimethyl-6-methylamino-pyrimidinium chloride; 20 μM), exerted a similar action on intraburst ISIs and period of fast ripple oscillations ($n = 5$).

These experiments demonstrate that changes in the fidelity of action potential timing in individual pyramidal cells are directly reflected in the amplitude and frequency of hippocampal fast-tripple oscillations. This is consistent with the idea that synchronous onset of individual pyramidal cell action potential bursts could represent a mechanism of fast ripple generation.

lp;&5q;1Synaptic mechanisms of fast ripple generation

The next series of experiments were designed to test the hypothesis that synchronous activation of recurrent collateral synapses in area CA3 was the mechanism responsible for synchronous onset of action potential bursts in individual pyramidal cells. Increasing the extracellular potassium concentration to 8.5 mM induced hypersynchronous burst of action potentials revealed by dual cell-attached recordings from neighboring CA3 pyramidal cells (Figs. 3, 4, 10). Bath application of selective AMPA-receptor antagonist 2,3-dioxo-6-nitro-1,2,3,4-tetrahydrobenzo[f]quinoxaline-7-sulfonamide (NBQX) (10 μM) and competitive NMDA-receptor antagonist D-(-)-2-amino-7-phosphonopentanoic acid (D-APV) (50 μM) desynchronized burst onset in neighboring pyramidal cells ($n = 6$) (Fig. 10*A*). The number of intraburst spikes in individual CA3 pyramidal cells progressively decreased from 5–20 to 3–10 spikes per burst, and burst duration progressively decreased by 63.3 ± 5.6% (from 73.2 ± 10.8 to 26.9 ± 6.4 msec; $n = 6$; $p = 0.006$) (Fig. 10*B*). The intraburst ISIs gradually increased by 10–50% (Fig. 10*B*). Time delay between two pyramidal cell burst onset progressively increased (Fig. 10*C*). After block of the glutamate AMPA and NMDA receptors, neighboring pyramidal cells demonstrated similar intraburst interspike intervals, but cross-correlation analysis of the intraburst spike timing between two pyramidal cells did not reveal any coherence attributable to random asynchronous bursts onset (Fig. 10*C*).

Simultaneous extracellular field potential recordings from the CA3 pyramidal cell layer revealed hypersynchronous population spikes during fast ripples (Fig. 11*A*,*B*). Bath application of the AMPA- and NMDA-receptor antagonists NBQX (10 μM) and D-APV (50 μM) desynchronized burst onset in individual pyramidal cells and rapidly and completely abolished large amplitude population field oscillations ($n = 16$) (Fig. 11*A*,*B*). Amplitude of burst-type discharges after suppression of AMPA and NMDA receptors varied from 10 to 250 μV, and spike width varied from 0.15 to 0.75 msec, corresponding to multiple unit activity (Fig. 11*B*). Power spectra amplitude in the fast ripple frequency range (200–600 Hz) decreased by 96 ± 0.9% ($n = 16$; $p = 7.9 \times 10^{-40}$). In the presence of ionotropic glutamate antagonists, burst-type discharges from multiple pyramidal cells were characterized by random nonsynchronous burst onset (Fig. 11*B*).

Thus, synchronous action potential burst onset mediated by recurrent excitatory synaptic transmission and similar intrinsic action potential timing in regional pyramidal cells determines the amplitude and frequency of fast ripple oscillations.

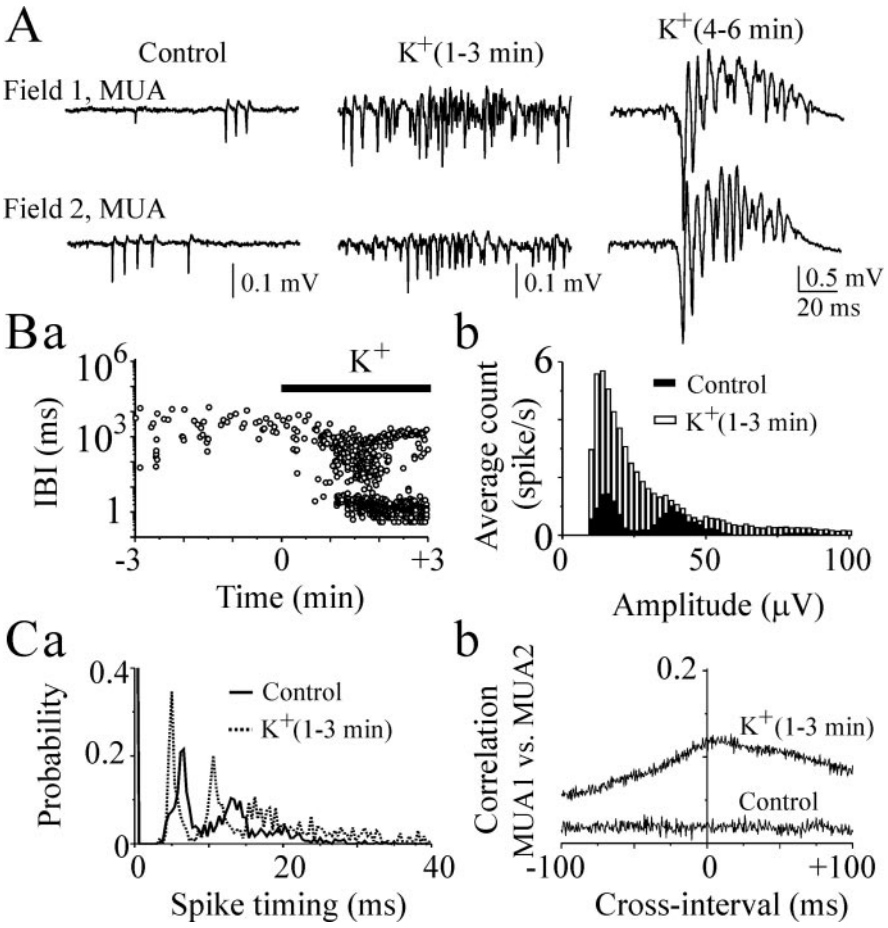

Figure 5. Transition from asynchronous action potentials to hypersynchronous population bursts. *A*, Examples of simultaneous extracellular field potential records of multiple unit activity and population activity from the CA3 pyramidal cell layer (sites are 200 μm apart) in a P20 rat hippocampal slice. In control, spontaneous asynchronous bursts of action potentials are present in both records. Bath application of 8.5 mM $[K^+]_o$ increased neuronal firing rate and burst synchronization, resulting in hypersynchronous network-driven population bursts. *Ba*,*b*, Effect of 8.5 mM $[K^+]_o$ on the interburst intervals and spike amplitudes (bin size, 2 μV). Interburst intervals progressively decreased after 8.5 mM $[K^+]_o$ application. Amplitude histograms for spontaneous multiple unit activity possessed several peaks in control conditions and were smoothed in the presence of 8.5 mM $[K^+]_o$. *Ca*, Intraburst ISIs decreased after 8.5 mM $[K^+]_o$ application (bin size, 0.4 msec). *Cb*, Cross-correlograms of MUA show their synchronization after 8.5 mM $[K^+]_o$ application.

Discussion

Our major finding is that high-frequency fast ripple oscillations in the hippocampus arise from the synchronous starting of a homogenous set of cellular oscillators. Glutamatergic synaptic transmission is necessary for the synchronous start, whereas intrinsic membrane conductances are responsible for the homogeneity of individual cellular oscillators. Our data do not exclude the possibility that feedback during FR contributes to the homogeneity of the oscillations. Thus, fast ripples are fundamentally a circuit phenomenon, although the basic timing mechanism determining the period of fast ripple oscillations is manifested at the level of a single neuron.

Spontaneous bursting activity in the hippocampus

Cellular bursting activity has been observed at many different levels of the nervous system, including thalamus, medial septum, and inferior olive, as well as other brainstem and forebrain regions (Llinas and Yarom, 1981; Jahnsen and Llinas, 1984a,b). A proportion of pyramidal cells in regions CA3 and CA1 of the hippocampus spontaneously generate bursts-type discharges characterized by random burst onset and high-frequency intraburst spikes. Burst-type discharges generated by regional pyramidal cells varied in number of spikes but were similar in the intraburst interspike intervals (Figs. 1, 2). Simultaneous whole-cell recordings from individual pyramidal cells and extracellular field potential recordings from the CA3 and CA1 pyramidal cell layer reveal stereotyped ISIs for individual neurones that varied up to $\pm$2 msec for different neurones within a local population. Morphology and electrophysiology of hippocampal pyramidal cells suggested that burst-type discharges are generated or modulated by ion channels on the apical dendrites (Bilkey and Schwartzkroin, 1990). Recent data suggest that in addition to intrinsic cellular mechanisms (Staff et al., 2000), synaptic activities contribute to the generation of spontaneous action potential bursts (Cohen and Miles, 2000; Szucs et al., 2003). In addition, the intrinsic burst pattern of individual hippocampal pyramidal cells depends on the interaction between glutamatergic and GABAergic receptor activity, representing a powerful mechanism of intraburst spike frequency modulation (Dzhala et al., 2003).

Hippocampal fast ripple oscillations

Fast ripples are interictal high-frequency oscillations in the 200–600 Hz range that can be recorded from limbic regions capable of generating spontaneous seizures in rodent models of epilepsy and in human medial temporal lobe epilepsy (Bragin et al., 1999a,b). We described similar patterns of hippocampal neuronal activity during high K^+-induced IEDs in hippocampal slices *in vitro* (Dzhala and Staley, 2003b). Spectral analysis of interictal epileptiform activity revealed a prominent increase of IED power in the frequency range of fast ripple oscillations preceding transition to ictal-like epileptiform activity (Dzhala and Staley, 2003b), and several studies demonstrated that focal seizures begin with high-frequency oscillations (Fisher et al., 1992; Bragin et al., 1999a; Traub et al., 2001).

Intrinsic membrane properties determine the period of fast ripple oscillations

Intrinsic cellular mechanisms underlie much of the spontaneous activity of pyramidal cells of the hippocampus *in vitro* (Cohen and Miles, 2000). Various combinations of ionic currents result in varying electrophysiological properties and patterns of intrinsic activity such as a regular spiking mode or a complex burst of action potentials (Connors and Gutnick, 1990). Spontaneous bursts recorded from the CA3 and CA1 subregions of the hippocampus varied in duration and number of intraburst spikes and intraburst interspike intervals but were characterized by stereotyped or similar intraburst interspike interval for different neurones within a local population (Figs. 1, 2). The correlation between the action potential of bursting pyramidal cells and local field potential oscillations suggests that simultaneous burst onset

and similar firing patterns in the regional pyramidal cells may be responsible for synchronous high-frequency network oscillations (Figs. 2, 6). Supporting this idea, manipulations that increased the homogeneity of spike timing in individual pyramidal cells, such as blocking spike train accommodation, dramatically increased the amplitude of fast ripple oscillations (Figs. 8, 9). On the other hand, manipulations that increased the heterogeneity of spike timing in individual pyramidal cells, such as blockade of I_{Kd}, substantially reduced fast ripple amplitude (Figs. 8, 9).

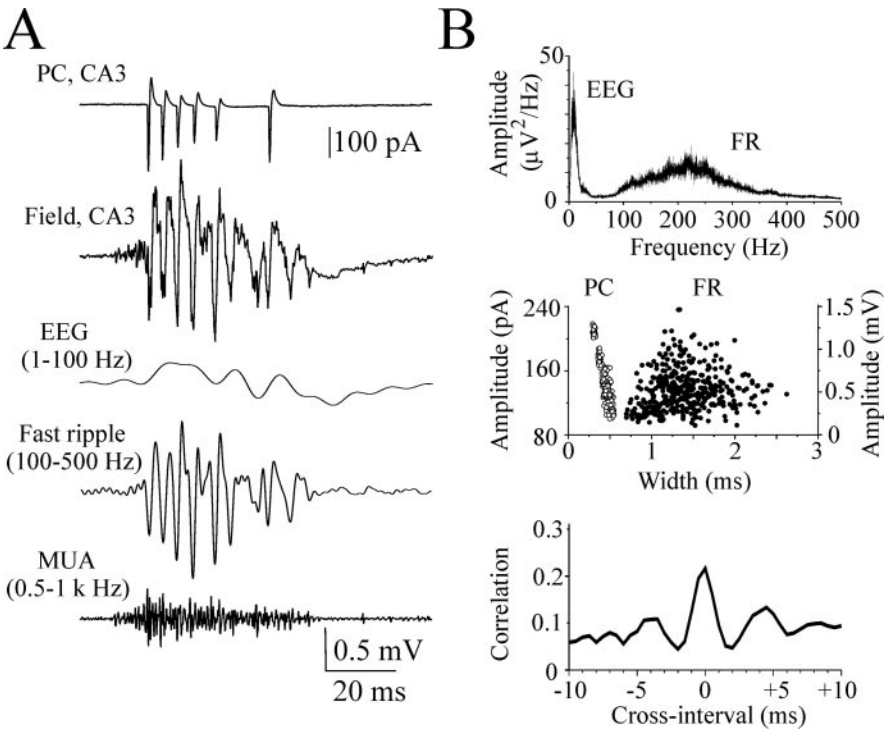

Figure 6. Fast ripple oscillations in the hippocampus. *A*, Example of population burst in hippocampal slice of P20 rat. Simultaneous cell-attached record from the CA3 pyramidal cell and nearby extracellular field potential record at the CA3 pyramidal cell layer before filtering (wide-band; 0.1 Hz–4 kHz) and after filtering for EEG component of population burst (bandpass; 1–100 Hz), population burst-related fast ripple (bandpass; 100–500 Hz), and MUA (high-pass; 500 Hz). *B*, Plots represent power spectra of population bursts (117 consecutive population bursts during 5 min record); amplitudes and widths corresponded to the CA3 pyramidal cell burst-type discharges (open circles; 668 spikes in 117 bursts) and population spikes related to the fast ripples (close circles; 1147 population spikes in 117 bursts); and cross-correlation histogram of FR related population spikes versus pyramidal cell discharges (bin size, 0.5 msec). Power spectra possesses two peaks corresponding to gamma frequency oscillations related to EEG band and 100–400 Hz oscillations related to fast ripples. Cross-correlogram shows coherent oscillations with a period of 3–6 msec.

Synaptic mechanism of fast ripple initiation

Numerous studies suggest a pivotal role of gap junctions in generation of fast ripple oscillations (Draguhn et al., 1998; Traub et al., 2001; Bikson et al., 2003; LeBeau et al., 2003), although none of the pharmacological or ionic manipulations of gap junction conductance is specific. We demonstrate that synchronous burst onset of the regional pyramidal cells mediated by recurrent excitatory synaptic transmission underlies the generation of hippocampal population burst and related fast ripple oscillations (Figs. 3–6, 10, 11). Specific and competitive antagonists of excitatory glutamatergic synaptic transmission completely abolished population bursts, suggesting that the primary mechanism of fast ripple initiation is synaptic (Figs. 10, 11).

We considered the extracellularly recorded bursts of action potentials (Fig. 1*A*) to arise from a single neuron based on the similarity of the spike widths and intervals to the spike widths and intervals obtained from cell-attached recordings (Fig. 1*Ac*,*B*). Although it is possible that those extracellular bursts were actually attributable to small groups of neurons whose activity was synchronized by gap junctions, their maximum amplitude was too low to represent a mechanism of fast ripple generation (Fig. 11*A*, *Bb*). Furthermore, the width of the extracellularly recorded spikes that we assumed to arise from single cells are an order of magnitude more narrow than the population spikes during synchronous network bursts (Fig. 1*Ab* vs Fig. 11) and fast ripples (Fisher et al. 1992; Bragin et al. 1999a,b).

Our data do not exclude the possibility that feedback mechanisms operant during the ripple may increase the homogeneity of spike timing during the ripple. Potential feedback mechanisms include glutamatergic recurrent excitatory synaptic activity or gap junctional excitation. However, such feedback is not sufficient to overcome normal spike train accommodation, nor is it sufficient to overcome increases in the variance of spike train timing induced by blockade or intrinsic potassium conductances. Thus, our data indicate that fast ripples can be most parsimoniously explained by recurrent excitation in area CA3, or afferent excitation in area CA1, leading to the synchronous initiation of a homogenous set of neuronal oscillators.

Recurrent excitation is increased in epileptogenic cortex and could provide the anatomical basis for fast ripple onset in epilepsy by providing a mechanism for the synchronous activation of neurons in the epileptic focus. Our data also suggest that alterations in intrinsic conductances are not necessary to observe fast ripples, consistent with the idea that such alterations are not necessary for epilepsy.

References

Abeles M, Gerstein GL (1988) Detecting spatiotemporal firing patterns among simultaneously recorded single neurons. J Neurophysiol 60:909–924.

Andersen P, Bliss TV, Skrede KK (1971) Unit analysis of hippocampal population spikes. Exp Brain Res 13:208–221.

Bikson M, Fox JE, Jefferys GR (2003) Neuronal aggregate formation underlies spatiotemporal dynamics of nonsynaptic seizure initiation. J Neurophysiol 89:2330–2333.

Bilkey DK, Schwartzkroin PA (1990) Variation in electrophysiology and morphology of hippocampal CA3 pyramidal cells. Brain Res 514:77–83.

Bragin A, Jando G, Nadasdy Z, Hetke J, Wise K, Buzsaki G (1995) Gamma (40–100 Hz) oscillation in the hippocampus of the behaving rat. J Neurosci 15:47–60.

Bragin A, Engel Jr J, Wilson CL, Fried I, Buzsaki G (1999a) High-frequency oscillations in human brain. Hippocampus 9:137–142.

Bragin A, Engel Jr J, Wilson CL, Fried I, Mathern GW (1999b) Hippocampal and entorhinal cortex high-frequency oscillations (100–500 Hz) in human epileptic brain and in kainic acid-treated rats with chronic seizures. Epilepsia 40:127–137.

Bragin A, Engel Jr J, Wilson CL, Vizentin E, Mathern GW (1999c) Electrophysiologic analysis of a chronic seizure model after unilateral hippocampal KA injection. Epilepsia 40:1210–1221.

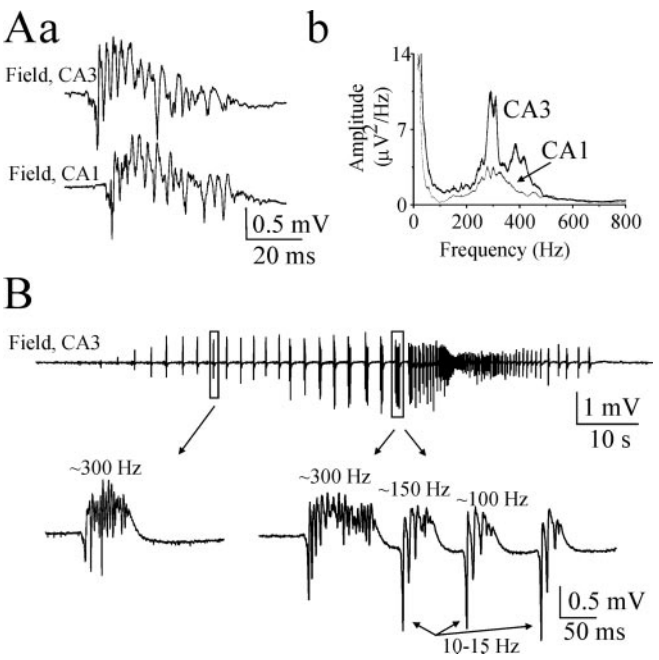

Figure 7. Spatial distribution of fast ripples and their properties before onset of ictal activity. *A*, Example of population burst simultaneously recorded from the CA3 and CA1 pyramidal cell layer in hippocampal slice of P22 rat. Population bursts were evoked by 8.5 mM $[K^+]_o$ bath application. Time delay between population burst onset indicates propagation of the population burst from area CA3 to CA1. Power spectrums of population bursts from the CA3 and CA1 ($n = 27$ population bursts) pyramidal cell layer reveal wider and higher FR frequency range in the CA3 area. *B*, Fast ripples before onset of ictal activity. Extracellular field potential recording (raw data, 0.1 Hz–4 kHz) was made in the CA3 pyramidal cell layer of P16 hippocampal slice. Extended parts show FR oscillations after onset of population bursts and before onset of ictal activity. FR amplitude increased after the appearance of population bursts. Before onset of ictal activity, FRs (200 – 400 Hz) followed by slower 100 –150 Hz oscillations and 10 –30 Hz secondary afterdischarges.

Bragin A, Mody I, Wilson CL, Engel Jr J (2002) Local generation of fast ripples in epileptic brain. J Neurosci 22:2012–2021.

Buzsaki G (1986) Hippocampal sharp waves: their origin and significance. Brain Res 398:242–252.

Cobb SR, Buhl EH, Halasy K, Paulsen O, Somogyi P (1995) Synchronization of neuronal activity in hippocampus by individual GABAergic interneurons. Nature 378:75–78.

Cohen I, Miles R (2000) Contributions of intrinsic and synaptic activities to the generation of neuronal discharges in *in vitro* hippocampus. J Physiol (Lond) 524:485–502.

Connors BW, Gutnick MJ (1990) Intrinsic firing patterns of diverse neocortical neurons. Trends Neurosci 13:99–104.

Draguhn A, Traub RD, Schmitz D, Jefferys JG (1998) Electrical coupling underlies high-frequency oscillations in the hippocampus *in vitro*. Nature 394:189–192.

Dzhala VI, Staley KJ (2003a) Excitatory actions of endogenously released GABA contribute to initiation of ictal epileptiform activity in the developing hippocampus. J Neurosci 23:1840–1846.

Dzhala VI, Staley KJ (2003b) Transition from interictal to ictal activity in limbic networks *in vitro*. J Neurosci 23:7873–7880.

Dzhala VI, Masino SA, Staley KJ (2003) Synaptic inputs modulate 100–250 Hz intrinsic code of hippocampal pyramidal cells. Soc Neurosci Abstr 29:810.11.

Fisher RS, Webber WR, Lesser RP, Arroyo S, Uematsu S (1992) High-frequency EEG activity at the start of seizures. J Clin Neurophysiol 9:441–448.

Jahnsen H, Llinas R (1984a) Electrophysiological properties of guinea-pig thalamic neurones: an *in vitro* study. J Physiol (Lond) 349:205–226.

Jahnsen H, Llinas R (1984b) Ionic basis for the electro-responsiveness and oscillatory properties of guinea-pig thalamic neurons *in vitro*. J Physiol (Lond) 349:227–247.

Jensen MS, Yaari Y (1997) Role of intrinsic burst firing, potassium accumulation, and electrical coupling in the elevated potassium model of hippocampal epilepsy. J Neurophysiol 77:1224–1233.

LeBeau FE, Traub RD, Monyer H, Whittington MA, Buhl EH (2003) The role of electrical signaling via gap junctions in the generation of fast network oscillations. Brain Res Bull 62:3–13.

Llinas R, Yarom Y (1981) Properties and distribution of ionic conductances generating electroresponsiveness of mammalian inferior olivary neurones *in vitro*. J Physiol (Lond) 315:569–584.

Madison DV, Nicoll RA (1986) Actions of noradrenaline recorded intracellularly in rat hippocampal CA1 pyramidal neurones, in vitro. J Physiol (Lond) 372:221–244.

McCormick DA (1990) Membrane properties and neurotransmitter actions. In: The synaptic organization of the brain (Sheherd GM, ed), pp 32–66. New York: Oxford UP.

Paxinos G, Watson C (1986) The rat brain in stereotaxic coordinates. San Diego: Academic.

Pedley TA (1980) Interictal epileptiform discharges: discriminating characteristics and clinical correlations. Am J EEG Technol 20:101–119.

Staff NP, Jung HY, Thiagarajan T, Yao M, Spruston N (2000) Resting and active properties of pyramidal neurons in subiculum and CA1 of rat hippocampus. J Neurophysiol 84:2398–2408.

Storm JF (1990) Potassium currents in hippocampal pyramidal cells. Prog Brain Res 83:161–187.

Szucs A, Pinto RD, Rabinovich MI, Abarbanel HD, Selverston AI (2003) Synaptic modulation of the interspike interval signatures of bursting pyloric neurons. J Neurophysiol 89:1363–1377.

Traub RD, Whittington MA, Buhl EH, LeBeau FE, Bibbig A, Boyd S, Cross H, Baldeweg T (2001) A possible role for gap junctions in generation of very fast EEG oscillations preceding the onset of, and perhaps initiating, seizures. Epilepsia 42:153–170.

Traynelis SF, Dingledine R (1988) Potassium-induced spontaneous electrographic seizures in the rat hippocampal slice. J Neurophysiol 59:259–276.

Vanderwolf CH (1969) Hippocampal electrical activity and voluntary movement in the rat. Electroencephalogr Clin Neurophysiol 26:407–418.

Ylinen A, Bragin A, Nadasdy Z, Jando G, Szabo I, Sik A, Buzsaki G (1995) Sharp wave-associated high-frequency oscillation (200 Hz) in the intact hippocampus: network and intracellular mechanisms. J Neurosci 15:30–46.

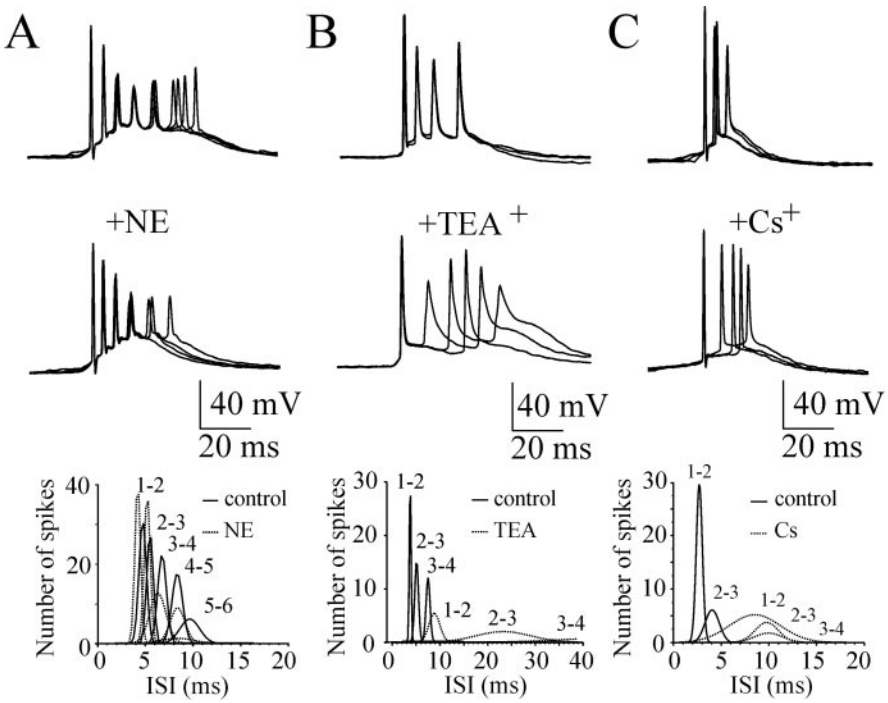

Figure 8. Contribution of intrinsic cellular properties to the intraburst ISIs. *A–C*, CA3 pyramidal cells were recorded in whole-cell current-clamp mode at the resting membrane potential. Superimposed traces represent spontaneous burst-type action potential activity in control (top traces) and after application of norepinephrine (NE; 20 μM), TEA^+ (2 mM), and Cs^+ (3 mM) (bottom traces). Plots below represent distribution of the intraburst ISIs in control and after drug applications (bin lag, 0.5 msec). ISIs were decreased after suppression of I_{AHP} and increased after I_{Kd} and I_h suppressions. A Gaussian probability distribution function was used to fit a curve to the active data plot.

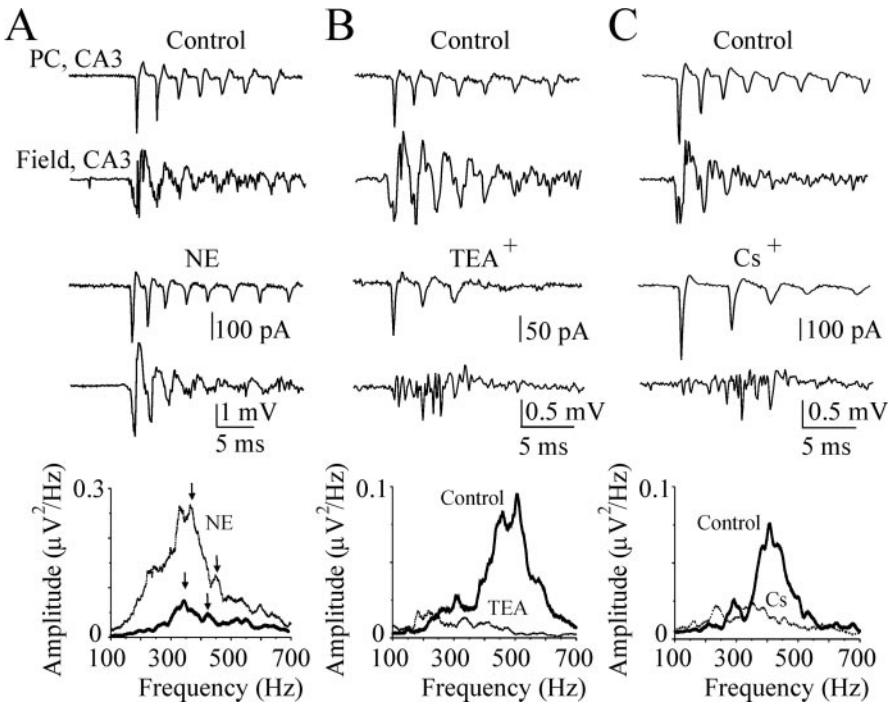

Figure 9. Contribution of intrinsic cellular properties to the timing of fast ripple oscillations. *A–C*, Examples of simultaneous cell-attached records from the CA3 pyramidal cells and nearby extracellular field potential records from the CA3 pyramidal cell layer in control (8.5 mM $[K^+]_o$) and after application of the I_{AHP} current blocker norepinephrine (20 μM), I_{Kd} current blocker TEA^+ (2 mM), and I_h current blocker Cs^+ (3 mM) in the P30 rat hippocampal slices. Plots below represent power spectrums in the fast ripple oscillation band before and after I_{AHP}, I_{Kd}, and I_h current blocker applications. Power spectra amplitude were increased after suppression of I_{AHP} and decreased after I_{Kd} and I_h suppressions.

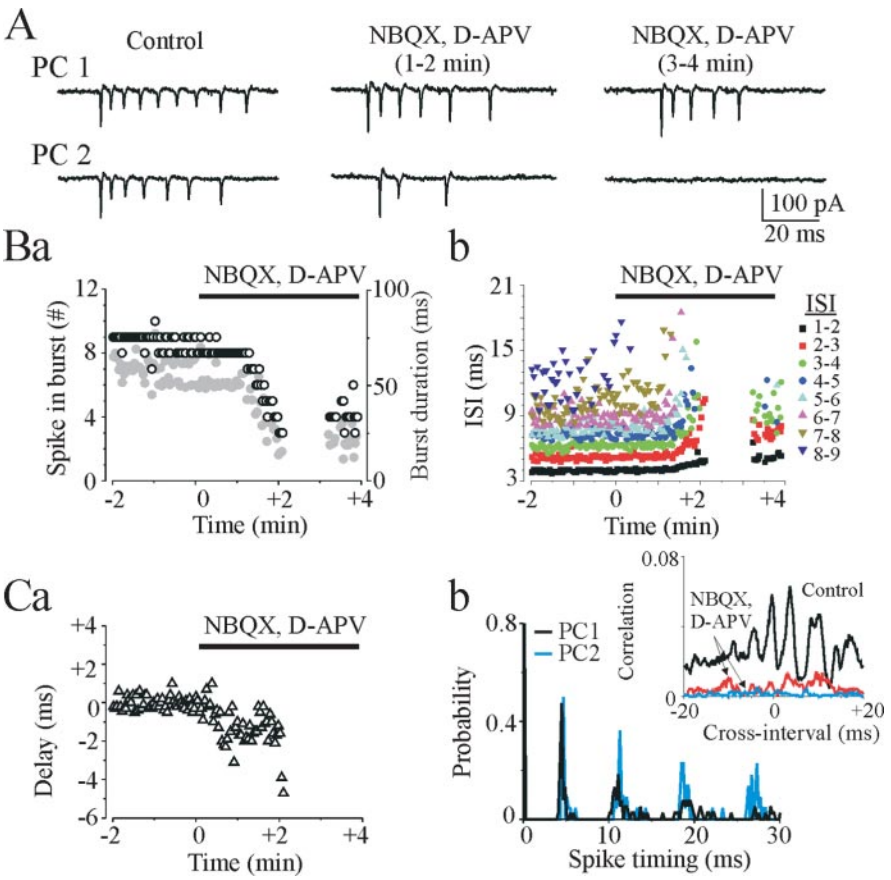

Figure 10. Effects of the glutamate receptor antagonist NBQX and D-APV on synchronous burst onset. *A*, Dual cell-attached recordings from neighboring CA3 pyramidal cells (PC1 and PC2) in a P18 rat hippocampal slice. Bath application of NBQX (10 μM) and D-APV (50 μM) decreased neuronal firing rate and increased time delay between bursts, resulting in their desynchronization. *Ba*,*b*, The number of intraburst spikes (white circles) and burst duration (gray circles) in the CA3 pyramidal cell (PC1) after NBQX and D-APV application progressively decreased, and ISIs progressively increased. *Ca*, Time delay between onset of bursts in two pyramidal cells in 8.5 mM $[K^+]_o$ progressively increased in NBQX and APV. *Cb*, Neighboring pyramidal cells after suppression of the glutamate AMPA and NMDA receptors exhibited similar intraburst interspike intervals (174 spikes, 37 bursts for PC1 and 147 spikes, 22 bursts for PC2; bin lag, 0.2 msec). Cross-correlation analysis of the intraburst spike timing in control (black line) reveals high-frequency oscillations with a period of 3–10 msec (100–350 Hz). Coherent oscillations are depressed (0–2 min; red line) and abolished (3–4 min; blue line) after NBQX and D-APV application.

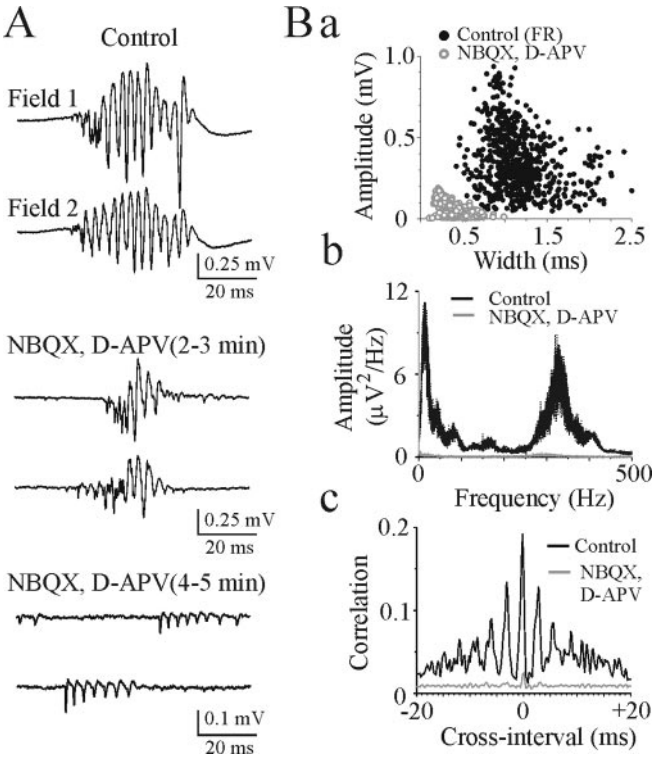

Figure 11. Effects on fast ripple oscillations of suppression synaptic excitation. *A*, Simultaneous extracellular field potential records of the population burst in the CA3 pyramidal cell layer of P22 rat hippocampal slice. Application of the AMPA- and NMDA-receptor antagonists NBQX (10 μM) and D-APV (50 μM) desynchronizes burst onset and completely abolishes population field oscillations induced by 8.5 mM $[K^+]_o$. *Ba*, Plots represent amplitude and width of the population spikes within fast ripples (close circles; 677 population spikes in 64 ripples) and amplitude and width of the burst-type discharges (open circles; 1005 spikes in 183 bursts) after suppression synaptic excitation. *Bb*, Power spectra of the extracellular field activity before and after suppression of synaptic excitation. Fast ripple oscillations (250 – 400 Hz) are abolished by blockade of AMPA and NMDA receptors. *Bc*, Cross-correlograms of extracellular population spikes evoked by 8.5 mM $[K^+]_o$ and multiple unit activity after suppression of population bursts by NBQX and D-APV (bin lag, 0.2 msec). Cross-correlograms show coherent oscillations with a period of 2.5– 4 msec in control and no correlation after suppression synaptic excitation.